Effect of Bonding on the Structure and Properties of Nanocellulose Films

Changbao Liang,[a] Jiayi Zhang,[a] Guohua Fu,[b] Zhiyang Jin,[c] Quanji Lu,[d] Xiaowen Li,[d] and Daran Yue [a],*

In this study, cellulose nanofibers (CNF) were obtained by chemical pretreatment using a rubberwood substrate. Different forms of drying were used to prepare three CNF film variants. Each of the films was rehydrated and hot-pressed to introduce more hydrogen bonds, and the films were characterized in terms of density and porosity, micromorphology, and mechanical properties. The mechanical properties of the films improved substantially after rehydration and hot-press drying. The tensile strengths of the films increased to approximately two to three times that of the original CNF films. These results with micromorphological observations suggest that adjusting the water content during CNF drying can significantly improve the formation of 3D networks in the films, thus imparting higher hydrogen bonding content to the films and improving the mechanical properties of the substrates. This study provides a theoretical basis for the formation of high-strength materials through water molecule-induced assembly and broadens the application of biomass cellulose materials in emerging fields.

INTRODUCTION

Since the beginning of the 21st century, with the surge in population, traditional single materials can no longer meet the requirements of developments in modern science and technology, making it increasingly important to prepare new composite materials from various raw materials (De Silva *et al.* 2015; Chen *et al.* 2019; Swolfs *et al.* 2019). Composite materials generally are comprised of a matrix combined with one or more reinforcing materials. The mechanical properties, biocompatibility, and chemical modification of the matrix material have a significant impact on the performance of the composite materials (Ray and Bousmina 2005). Matrix materials are typically divided into organic and inorganic materials. Conventional inorganic carrier materials usually use ions as precursors. Powder particles are obtained in the form of classical crystal nucleation and growth *via* electrostatic interactions between ions (Thanh *et al.* 2014; Karthika *et al.* 2016). These ionic compounds do not have structural continuity and shape controllability, and they are poorly biocompatible and hard to degrade. In contrast, organic materials usually

use organic monomers as precursors, which are covalently bonded to form a linear or reticular structure. This mode can easily realize not only the plastic preparation of continuous structural materials but also allow the polymerization and cross-linking between monomers, resulting in materials with high mechanical strength. Among them, cellulose, which has good bioactivity and mechanical strength, is widely used as an organic backbone support carrier to load inorganic particles and nanoparticles to prepare multifunctional composites with additional properties (Fu *et al.* 2018; Jiang *et al.* 2018; Li *et al.* 2019).

Cellulose, a straight-chain polymer compound consisting of β-D-glucopyranosyl groups linked by β-1,4-glycosidic bonds, has been relevant to human lives since ancient times; it has been used as building materials, clothing, and chemical raw materials (Klemm *et al.* 2005; Habibi *et al.* 2010; Habibi. 2014). Among the many cellulose-derived materials, nanofibrillated cellulose offers a unique natural advantage as an organic backbone support material for effective combination with nanoparticles, polymers, and biomolecules because of its high Young's modulus, high strength, ultra-fine structure, and specific surface area (Klemm *et al.* 2011; Moon *et al.* 2011; Thomas et al. 2018). Song *et al.* (2017) used cellulose nanofibers (CNF) as a carrier and prepared 40 groups of CNF with reduced graphene oxide (RGO) films having thermal conductivities of $\lambda_x/\lambda_z = 279$. It was found that one-dimensional CNF and two-dimensional reduced graphene oxide films exhibited good synergistic mechanical properties with excellent flexibility and high tensile strength (107 MPa). Hou *et al.* (2018) prepared CNF/RGO conductive paper with an RGO mass fraction of 4% using chemical treatment and vacuum filtration, whose electrical conductivity was as high as 4382 S/m and tensile strength (90.9 MPa) was relatively close to that of pure CNF paper (109.1 MPa). Yan *et al.* (2014) prepared a nanocellulose/graphene composite nanopaper that was still able to sense in all directions under 100% stretching conditions, and its strength was more than 10 times higher than that of stretchable carbon nanotube and silver nanowire sensors, making it an ideal material for testing dynamic indicators. Huang *et al.* (2015) designed a nanocellulose network using nanosheets and then prepared highly conductive composite nanocellulose aerogels with electromagnetic shielding effectiveness of up to 219 dB cm^3/g for specific ethylene sulfate-1-methyl-3-ethylimidazole (EMI SE), which has great potential for application in spacecraft and special weapon materials. Cellulosic nanofibers contain a large number of hydroxyl groups, a high specific surface area, and good mechanical properties, which make them ideal environmental carriers for the preparation of multifunctional composites (Islam *et al.* 2014; Ling *et al.* 2018a).

Nanocellulose is an excellent high-strength support and carrier material, which is attributed to its high polarity and ability to produce strong hydrogen bonding easily (Benitez *et al.* 2013; Ling *et al.* 2018b). The large number of intramolecular hydroxyl groups facilitates the formation of hydrogen bonds within and between cellulose molecular chains during evaporative drying due to capillary forces (Parthasarathi *et al.* 2011; Buchtova and Budtova 2016; Wu *et al.* 2020). In turn, during the formation of hydrogen bonding-induced nanocellulose-based high-strength support carrier materials, water molecules become important participants in the construction of hydrogen-bonding network structures. Therefore, humidity and moisture content have a major influence on the formation of nanocellulose-based hydrogen-bonded network structures (Verho *et al.* 2013). To date, there have been only a few reports on water molecule-induced nanocellulose assembly to build high-strength support carrier materials. Revealing the role of water

molecules in the drying process of nanocellulose-based materials has a profound impact on improving the mechanical properties of carrier materials.

In this study, a method was designed to investigate ways in which water molecules affect the structure and properties of nanocellulose films by various drying methods (natural drying, freeze-drying, and replacement drying) with nanocellulose as the substrate. Specifically, CNF was prepared using a chemo-mechanical method using rubber wood (RW) as the raw material. Fourier infrared spectroscopy, X-ray diffraction, thermogravimetric analysis, and scanning electron microscopy were used to characterize and analyze the nanocellulose filaments. In order to explore more deeply the effect of water molecules on the film structure under the synergistic effect of hydrogen bonding during the drying of nanocellulose films, the extracted CNF films were subjected to natural drying, freeze-drying, and alternative drying treatments. In Furthermore, water molecules are believed to play an important role in the film structure and properties during drying. The dried films were rehydrated and then subjected to high-temperature hot pressing to investigate the changes in film properties before and after hot pressing as a way to reveal the hypothesis of hydrogen bond formation between fibers due to contraction from capillary forces during drying. In addition, the effects of water molecules on the mechanical properties of nanocellulose films were investigated by characterizing their microscopic morphology and mechanical properties.

EXPERIMENTAL

Materials

The RW was obtained from Danzhou City (Hainan, China), and was cut with a plant crusher to produce a 40 to 60 mesh powder. Benzene (AR, 99.5%), anhydrous ethanol (ACS, 99.5%), potassium hydroxide (AR, 85%), sodium chlorite (80%), and acetic acid (99.8%) were provided from Damao Chemical Reagent Co. Ltd. (Tianjin, China).

Experimental Methods

Isolation of CNFs

The CNFs were prepared from RW, as reported in the literature (Abe and Yano 2009). Briefly, 2 g of RW was placed in a Soxhlet apparatus, and an appropriate amount of benzene-alcohol solution (benzene:ethanol = 2:1; v/v) was added, and extracted in a water bath at 95 °C for 6 h to remove fatty acids and terpenoids. Thereafter, the extracted RW was placed in a conical flask containing 65 mL of distilled water, and 0.6 g of sodium chlorite and 0.5 mL of glacial acetic acid were added. The contents were heated in a constant temperature water bath at 75 °C for 1 h. This process was repeated 4 to 5 times. Immediately thereafter, the sample from the previous step was treated with 100 mL of potassium hydroxide solution (5 wt%) for 2 h to remove hemicellulose. The product obtained was named purified cellulose fiber (PCF). The PCF was treated in an ultrasonic cell crusher for 30 min (1 s interval, 1 s working) to obtain CNF. The PCF and C0000NF were freeze-dried and stored in a desiccator.

Fabrication of nanocellulose films

A certain amount (0.04 g) of CNF was prepared in a suspension with a concentration of 0.3% and passed through a sand core filter to form a CNF gel on the filter membrane. The CNF gel then underwent natural drying, freeze-drying, or displacement

drying. For natural drying, the CNF gel was allowed to dry naturally in a fume hood (room temperature is 25±3 °C) until it reached a constant weight and was recorded as AD-CNF. For freeze-drying, the CNF gels were freeze-dried at -20 °C for 24 h and then transferred to a vacuum freeze dryer at 0.1 Pa for 24 h and recorded as FD-CNF. For displacement drying, the CNF gels were immersed in 25% tert-butanol/water solution for 12 h at room temperature (25±3 °C). This process was then repeated with 50%, 70%, and 100% tert-butanol/water solution. The gels were then dried naturally to a constant weight and recorded as SD-CNF. After reaching a constant weight, all samples were dried at 105 °C for 24 h to remove the adsorbed water from the CNF film and then stored in a desiccator. The obtained films had a thickness of approximately 50 to 100 μm.

Rehydration and hot-press drying of nanocellulose films

To introduce more hydrogen bonds into the CNF films, they were immersed in distilled water at room temperature (25±3 °C) for 24 h to reach saturation point in terms of water content. The water-saturated CNF films were then transferred to a hot press at 120 °C and 0.5 MPa for 3 min to obtain rehydrated and hot-press-dried nanocellulose films, which were referred to as RAD-CNF, RFD-CNF, and RSD-CNF, respectively.

Characterization

Characterization of fibers

The morphologies of RW, PCF, and CNF were visualized using a scanning electron microscope (SEM, Zeiss Merlin Compact, Oberkochen, Germany). All the samples were sprayed with gold. A Fourier-transform infrared spectrometer (FTIR, Nicolet, Madison, WI, USA) was used to describe the changes in the chemical structure during CNF preparation. The spectra were recorded in the range of 400 to 4000 cm^{-1}. The crystallinities of RW, PCF, and CNF were analyzed by X-ray diffraction (XRD, D/max 2200, Rigaku, Japan). The scanning range was 5 to 60° with a scanning speed of 5 °/min. The crystallinity index (X_c) values of the samples were calculated using the Segal method (Segal *et al.* 1958). The thermal stabilities of RW, PCF, and CNF were studied using a thermogravimetric analyzer (TG, TGA5500 type, New Castle, DE, USA). Thermograms were acquired between 30 and 800 °C at a rate of 10 °C/min.

Characterization of cellulose nanofilms

The density of the nanocellulose film was calculated using the following equation,

$$\rho = \frac{m}{v}$$

(1)

where ρ is the density, *m* is the mass (g), and *v* is the volume (cm^3). To accurately determine the film thickness, a thickness gauge was used to measure the thickness at ten different locations and the average value was used as the film thickness.

The porosity of the nanocellulose films was calculated using Eq. 2,

$$D = (1 - \frac{\rho_a}{\rho_c}) \times 100$$

(2)

where *D* is the porosity (%), ρ_a is the CNF film density (g/cm^3), and ρ_c is the cellulose density [$\rho_c = 1.5\ g/cm^3$ (Yang *et al.* 2019)].

The mechanical properties of all films were characterized using an electronic universal testing machine (CMT6103 type). The specimen used was 20 mm long and 5 mm

wide. The specimens were extended at 5 mm/min and three measurements were made per group. The micromorphology was observed using a SEM for surface micromorphology and tensile sectioning.

RESULTS AND DISCUSSION

Extraction of CNFs

The CNFs were prepared by chemical pretreatment combined with ultrasonic treatment (Fig. 1a). The initial RW material was composed of cellulose, lignin, and hemicellulose components, with dense intercellular connections and a smooth surface (Fig. 1b). After chemical treatment, the fibers in the PCF were separated from each other and the cell walls were thinned, indicating that "gluing" components, such as lignin and hemicellulose, had been removed (Fig. 1c). With further sonication, the size and morphology of the obtained CNFs were considerably different from those of RW and PCF, with nanoscale fibers and a high aspect ratio (Fig. 1d). The CNFs were interwoven to form a mesh structure, which provided strong conditions for the subsequent preparation of nanocellulose films.
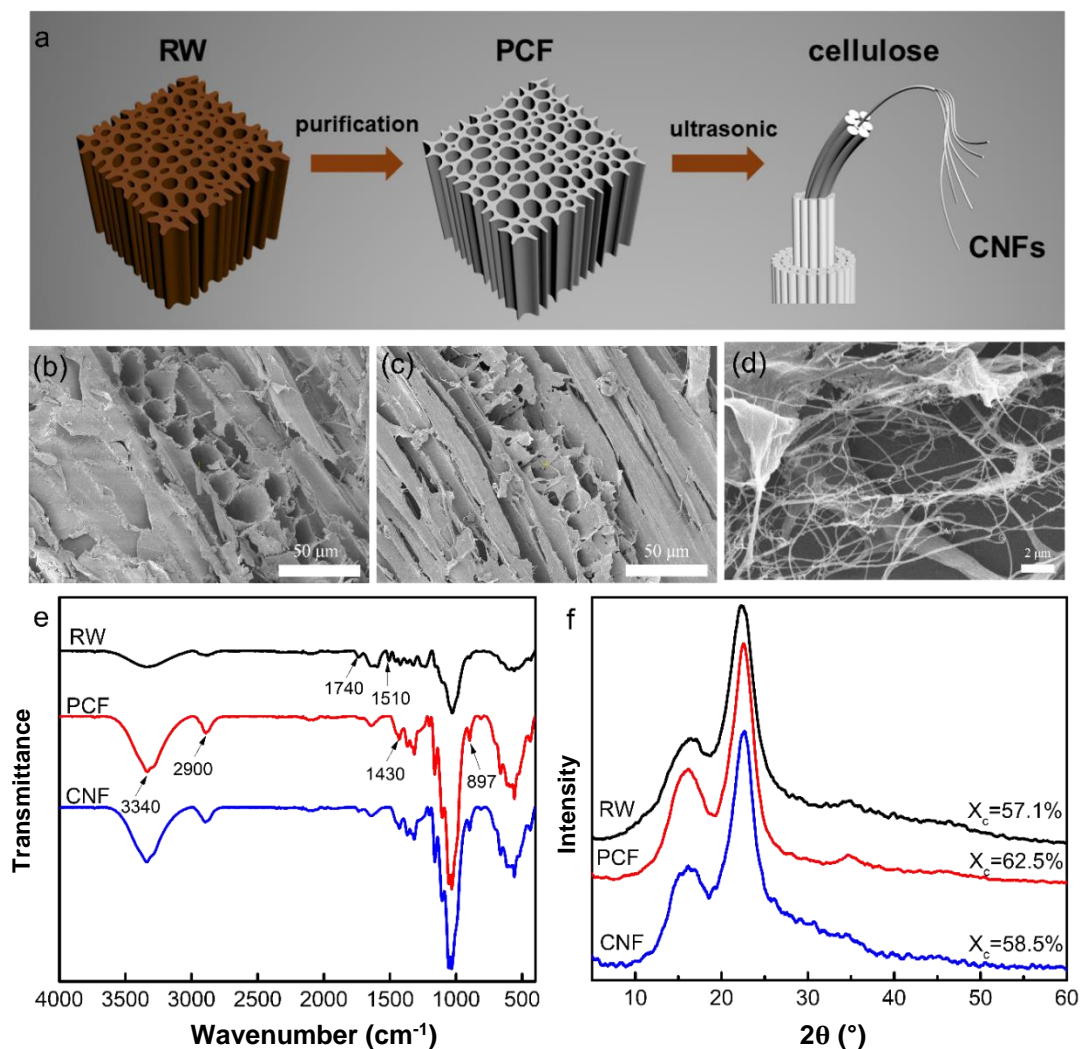
Fig. 1. (a) Isolation schematic of cellulose nanofibers (CNFs); (b-d) SEM images of rubberwood (RW), purified cellulose fiber (PCF), and CNFs; (e) FTIR spectra of RW, PCF, and CNFs; and (f) XRD curves of RW, PCF, and CNFs

Fourier transform infra-red spectroscopy is an important tool for characterizing the changes in chemical functional groups during the preparation of nanocellulose. Figure 1e shows the chemical structure changes during the preparation of the CNFs. The characteristic peaks at 1740 and 1510 cm^{-1} in RW correspond to the stretching vibrations of the hemicellulose polyxylose chromogenic group and C=C of the benzene ring skeleton in lignin, respectively. After chemical treatment, the characteristic peaks at 1740 cm^{-1} and 1510 cm^{-1} disappeared, indicating that hemicellulose and lignin were largely removed (Abou *et al.* 2009). In addition, the peaks characteristic cellulose peaks were present throughout the chemical treatment, with intense peak at 3340 cm^{-1} attributed to the stretching vibration of –OH, the peak at 2900 cm^{-1} due to the stretching vibration of –CH, the characteristic peak at 1430 cm^{-1} corresponding to the internal bending vibration of –CH$_2$ with –OCH, and peak at 897 cm^{-1} due to the vibration of anomeric carbon, indicating that cellulose was not affected (Wu *et al.* 2019).

Figure 1f shows the changes in the crystalline structure during the extraction of the CNF. All samples showed diffraction peaks around 16.5° and 22.6°, indicating a typical cellulose type I structure. This shows that the crystal structure of cellulose was not altered during chemical treatment (Wu *et al.* 2019). The relative crystallinity of RW was 57.1% and that of PCF obtained after treatment with sodium chlorite and potassium hydroxide increased by 62.5% owing to the removal of lignin and hemicellulose. However, the relative crystallinity of the CNF obtained after sonication was 58.5%, which was a slight reduction. This might have been caused by the damage to some crystalline regions of cellulose due to the cavitation produced during the ultrasonic process.
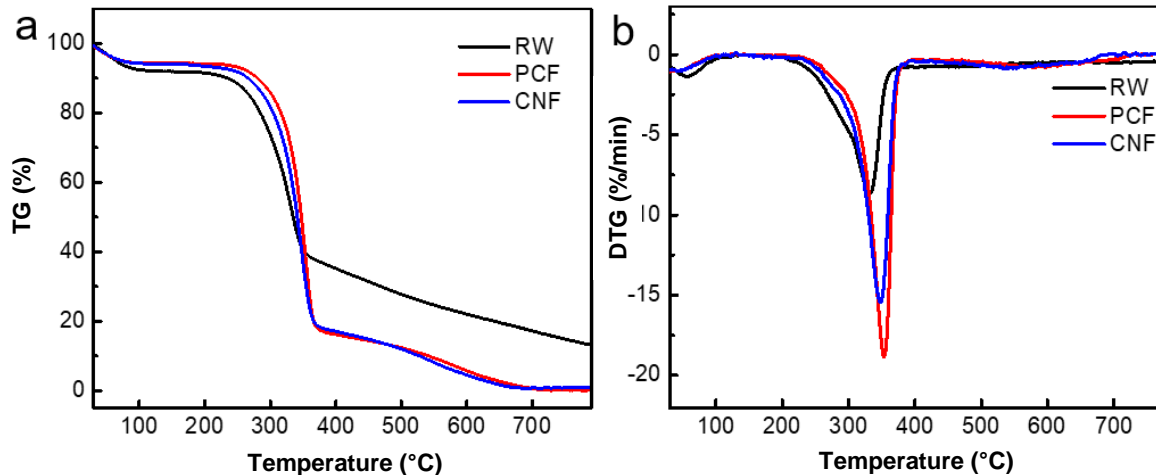

Fig. 2. Thermogravimetric (TG) and differential thermogravimetric (DTG) curves of RW, PCF, and CNF

Figure 2 shows the thermogravimetric (TG) and differential thermogravimetric (DTG) curves for RW, PCF, and CNF. As can be observed from Fig. 2, all samples showed a slight loss of mass in the range of 30 to 150 °C during the initial stages of warming. This was due to the evaporation of the adsorbed water retained in the sample as the temperature increased. As the temperature continued to rise, the maximum rate of weight loss was reached at 331.96 °C, 353.41 °C, and 348.24 °C for RW, PCF, and CNF, respectively. The higher temperature of maximum weight loss rate of PCF compared to RW can be attributed to the removal of the less thermally stable hemicellulose (which degrades at approximately

180 to 350 °C) (Poletto *et al.* 2012). The reduction in the maximum CNF weight loss rate temperature after sonication may be attributed to the destruction of the cellulose crystalline region during sonication, resulting in a reduction in its thermal stability which is consistent with the XRD test results. Above 350 °C, the RW mass residue is consistently higher than that of PCF and CNF, due to the higher thermal stability of lignin, which consists of three benzene-propene type unit structures that are highly cross-linked (John and Thomas 2008).

Mechanical Properties of Thin Films Related to Bonding

In this study, a three-step process was used to investigate the effect of bonding on the structural properties of CNF films. First, the CNFs were prepared by chemical pretreatment and sonication. Three different drying methods were immediately used to explore the effect of water molecules on the structure of the prepared nanocellulose films. Finally, a rehydration treatment coupled with mechanical hot pressing was used on the films to increase the inter-fiber contact area, resulting in entanglement as well as the introduction of more hydrogen bonds. The CNF films prepared by the three drying methods showed substantial structural differences. Figure 3 shows digital photographs of their surface microscopic morphology. The AD-CNF films (naturally dried) had smooth surfaces and dense textures.
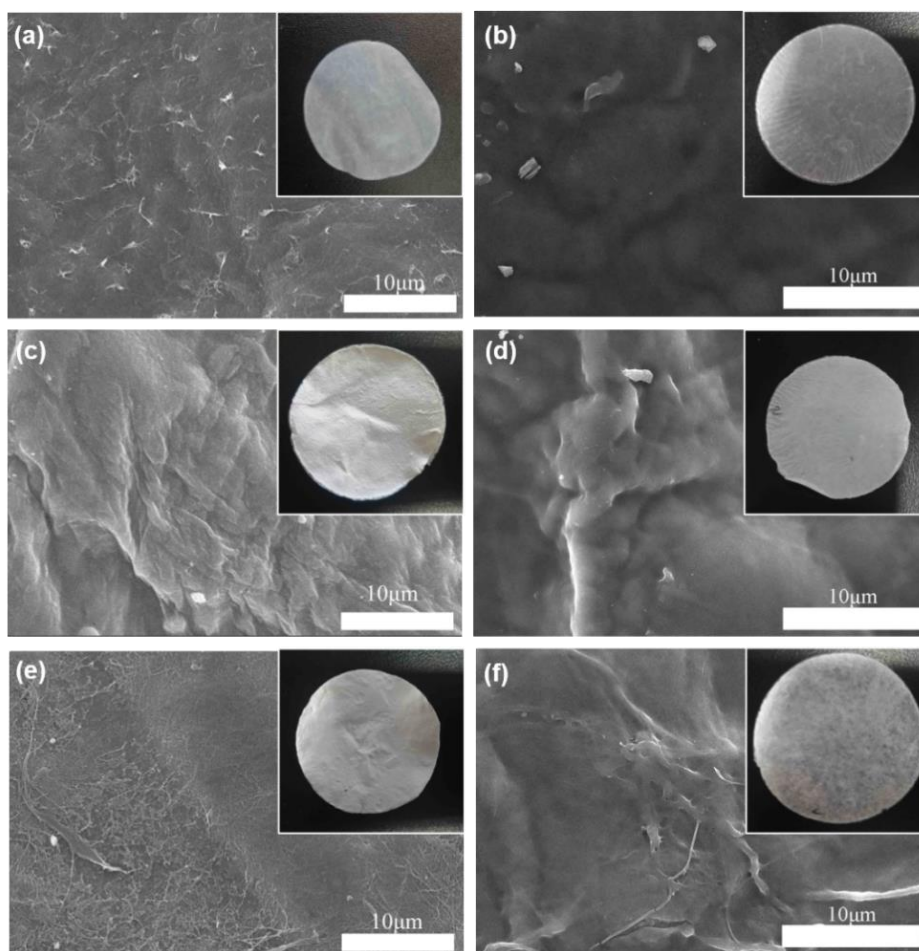

Fig. 3. Thin film SEM images of (a) AD-CNF; (b) RAD-CNF; (c) FD-CNF; (d) RFD-CNF; (e) SD-CNF; and (f) RSD-CNF. The inset shows a macro photograph of the films.

During natural drying, the evaporation of water molecules leads to the replacement of the original "cellulose-water-cellulose" hydrogen bonds with "cellulose-cellulose" hydrogen bonds within the fibers. The AD-CNF films exhibited the highest density ($\rho = 0.54$ g/cm^3) and lowest porosity ($D = 64.29\%$). This is also clearly demonstrated in the SEM image (Fig. 3a), where the fibers are more closely aligned with each other. During the freezing of FD-CNF, the freezing of water molecules to form ice crystals prevented the surface from being close enough to allow the formation of binding at the molecular level (Benitez *et al.* 2013). The growth of ice crystals during drying drives the CNF assembly to form a lamellar structure (Fig. 3c), resulting in its lower density ($\rho = 0.44$ g/cm^3) and higher porosity (D = 70.38%). Tertiary butanol is often used as a displacing agent owing to its high freezing point and low surface tension. During the *tert*-butanol displacement process, the water molecules in the original network structure were replaced by *tert*-butanol, which greatly reduced the destruction of the fiber network structure during drying. This restricted the formation of bonds between the CNFs, resulting in a rough surface and loose structure of SD-CNF with a large number of gaps between the fibrils (Fig. 3e) (Han *et al.* 2019). The SD-CNF exhibited the lowest density ($\rho = 0.34$ g/cm^3) and highest porosity (D = 77.60%).

Table 1. Density and Porosity Before and After Hot-Pressing

| Drying Method	Initial Density (g/cm^3)	Density after Hot-pressing (g/cm^3)	Initial Porosity (%)	Porosity after Hot-pressing (%)	Porosity Reduction Rate (%)
Natural	0.54	0.70	64.29	53.22	17.23
Freeze	0.44	0.64	70.38	57.29	18.60
Displacement	0.34	0.66	77.60	55.78	28.12

The mechanical properties were further investigated based on the microscopic morphology and structure (Fig. 4). The difference in mechanical properties in Fig. 4 is a visual indication of the effect of water molecule-induced bond formation on the structure of the CNF films.
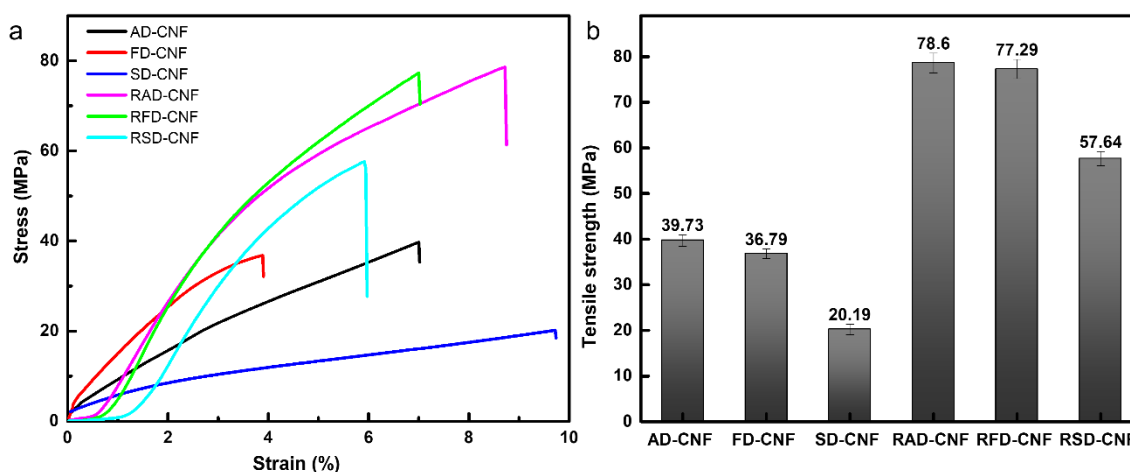
Fig. 4. Mechanical properties of films: (a) Stress–strain; and (b) Tensile strength

The presence of hydroxyl groups between fibrils is thought to be the basis for the formation of hydrogen bonds. At the same time, the formation of hydrogen bonds promotes the entanglement of nanocellulose particles with each other, which coordinates with each

other to further improve the mechanical strength of the film. It was found that the tensile strength of AD-CNF was approximately twice that of SD-CNF, suggesting that water molecules play the role of an "adhesive" in the assembly of the film, facilitating the formation of the hydrogen-bonding network structure.
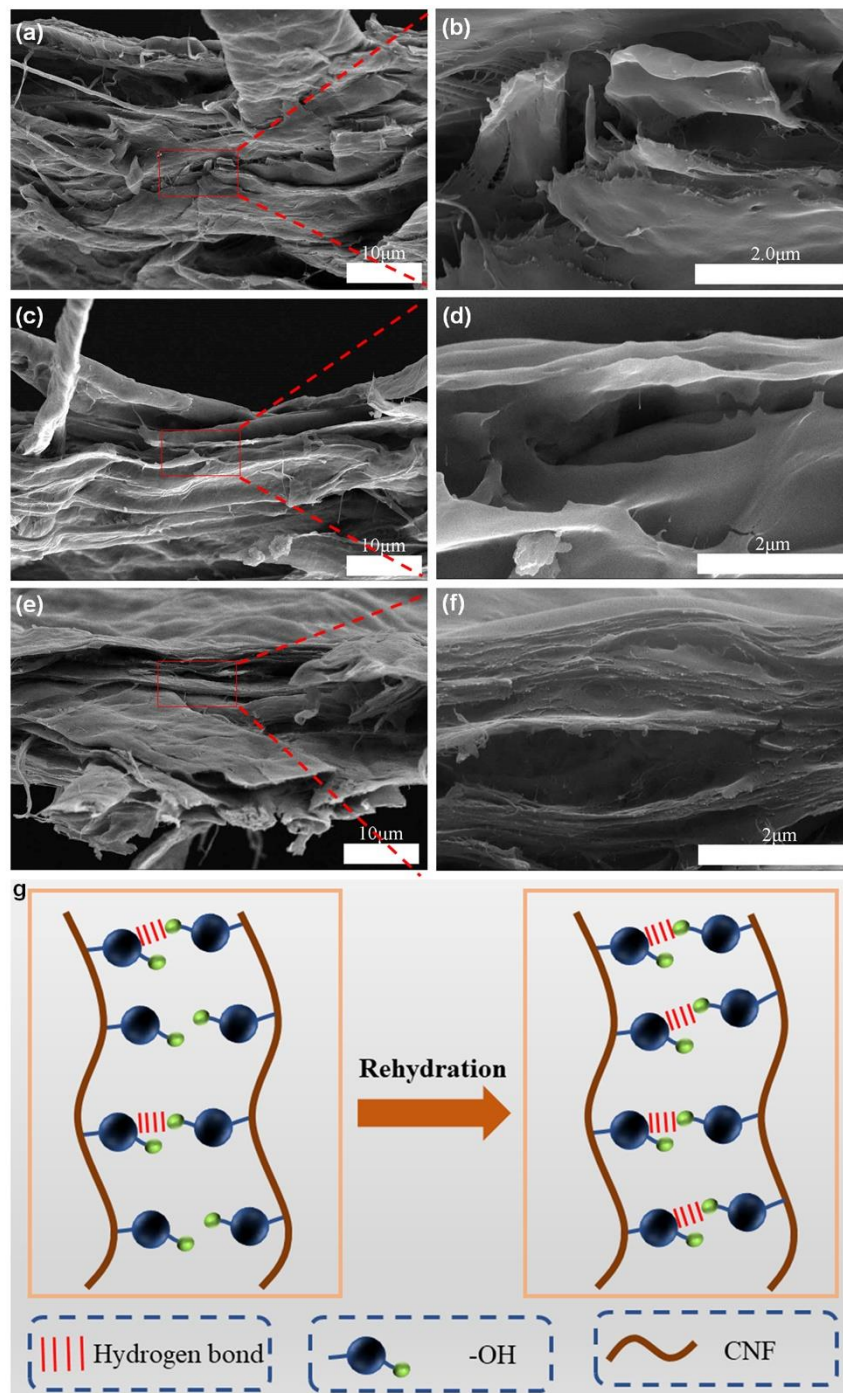
Fig. 5. Hot-pressed CNF-film tensile sections: (a, b) RAD-CNF; (c, d) RFD-CNF; (e, f) RSD-CNF; and (g) Schematic illustration of the rehydration and hot-press drying procedure

CNFs exhibit a high degree of water absorption owing to the large number of hydroxyl groups on their surface. To further investigate the effect of bonding on the

structure and properties of the CNF films, the three CNF films were rehydrated combined with mechanical hot-pressing treatment. The water molecules introduced by the rehydration and hot-press drying treatment allowed the formation of a large number of hydrogen bonds in the network structure of the fibril assembly. At the same time, the pressure helped the cellulose to overcome its inherent spatial resistance, while the temperature provided by the hot pressing process softened the cellulose and promoted interfibrillar entanglement under capillary pressure, forming an increasingly "strong" three-dimensional network (Hossain *et al.* 2021). Table 1 shows that regardless of the drying method used, the density and porosity changed considerably during hot-pressing. Although the density and porosity of the films fabricated using the three drying methods tended to be similar, RAD-CNF still exhibited a higher density ($\rho = 0.70$ g/cm^3) and lower porosity ($D = 53.22\%$) than the other two films, and was denser and smoother after hot pressing. In addition, SD-CNF exhibited the greatest change, with a 28.12% reduction in porosity. Figure 3f clearly shows that there were no significant fibrils in the CNF films after hot-pressing.

The contribution of the thermal pressure to bond formation was visually confirmed by the mechanical properties (Fig. 4). After hot-pressing, the tensile strengths of the RAD-CNF and RFD-CNF films were approximately twice as large as they were before hot-pressing, while the tensile strength of the RSD-CNF film was approximately three times as large. RSD-CNF is more likely to form a relatively dense three-dimensional structure after hot pressing due to its larger fiber spacing. This was further confirmed by the tensile strength results obtained after hot-pressing (Fig. 5). The RAD-CNF film has a relatively neat section and is assembled into a lamellar structure that is mostly pulled off during stretching, whereas the RFD-CNF film has a partial fibril structure, indicating that some of the fibrils are withdrawn during stretching. The RSD-CNF film is mostly lamellar and uneven, which may be attributed to its low hydrogen bonding content and weaker bonding between fibrils and microfibrils. Furthermore, the fibrils slide during stretching; therefore, their tensile strength is low. In brief, the inter-nanocellulose entanglement effect was further improved by rehydration and hot pressing, thus significantly improving the mechanical properties of the films (Fig. 5g).

CONCLUSIONS

1. The cellulose nanofibers (CNF) were successfully prepared by chemical pretreatment and ultrasonication to remove components such as lignin and hemicellulose from the rubber wood (RW) raw material. The prepared CNFs exhibited good thermal stability and crystalline properties.
2. Three CNF films, air-dried (AD-CNF), freeze-dried (FD-CNF), and displacement dried (SD-CNF), were prepared using natural drying, freeze-drying, and solvent displacement drying, respectively. The three films were characterized by their density and porosity, micromorphology, and mechanical properties. Comparing the characteristics of the AD-CNF, FD-CNF, and SD-CNF films, they exhibited a decrease in density, increase in porosity, and decrease in mechanical properties. These results combined with micromorphological observations confirmed that water molecules play an active role in the formation of bonded network structures and facilitate the assembly of CNF films.

3. The three films prepared were rehydrated and hot-pressed, and their tensile strengths increased to approximately 2 to 3 times of the initial tensile strength. It was further shown that bonding has a significant influence on the structure and properties of CNF films, revealing the changes in the intrinsic structure of bonding during the assembly of CNF films.

4. This study aimed to reveal the effect of bonding on the structure and properties of CNF films by controlling the drying method to regulate the formation of a bonding network structure using CNFs as the substrate. This research provides a theoretical basis for the application of biomass cellulose materials in emerging fields.

ACKNOWLEDGMENTS

REFERENCES CITED

Abe, K., and Yano, H. (2009). "Comparison of the characteristics of cellulose microfibril aggregates of wood, rice straw and potato tuber," *Cellulose* 16(6), 1017-1023. DOI: 10.1007/s10570-009-9334-9

Abou Taleb, M. F., El-Mohdy, H. L. A., and El-Rehim, H. A. A. (2009). "Radiation preparation of PVA/CMC copolymers and their application in removal of dyes," *Journal of Hazardous Materials* 168(1), 68-75. DOI: 10.1016/j.jhazmat.2009.02.001

Benitez, A. J., Torres-Rendon, J., Poutanen, M., and Walther, A. (2013). "Humidity and multiscale structure govern mechanical properties and deformation modes in films of native cellulose nanofibrils," *Biomacromolecules* 14(12), 4497-4506. DOI: 10.1021/bm401451m

Buchtova, N., and Budtova, T. (2016). "Cellulose aero-, cryo- and xerogels: Towards understanding of morphology control," *Cellulose* 23, 2585-2595. DOI: 10.1007/s10570-016-0960-8

Chen, Y., Dang, B., Jin, C., and Sun, Q. (2019). "Processing lignocellulose-based composites into an ultrastrong structural material," *ACS Nano* 13(1), 371-376. DOI: 10.1021/acsnano.8b06409

De Silva, R., Vongsanga, K., Wang, X., and Byrne, N. (2015). "Development of a novel regenerated cellulose composite material," *Carbohydrate Polymers* 121, 382-387. DOI: 10.1016/j.carbpol.2014.12.018

bioresources.com

Fu, Q., Ansari, F., Zhou, Q., and Berglund, L. A. (2018). "Wood nanotechnology for strong, mesoporous, and hydrophobic biocomposites for selective separation of oil/water mixtures," *ACS Nano* 12(3), 2222-2230. DOI: 10.1021/acsnano.8b00005

Habibi, Y. (2014). "Key advances in the chemical modification of nanocelluloses," *Chemical Society Reviews* 43(5), 1519-1542. DOI: 10.1039/c3cs60204d

Habibi, Y., Lucia, L. A., and Rojas, O. J. (2010). "Cellulose nanocrystals: Chemistry, self-assembly, and applications," *Chemical Reviews* 110(6), 3479-3500. DOI: 10.1021/cr900339w

Han, X., Ye, Y., Lam, F., Pu, J., and Jiang, F. (2019). "Hydrogen-bonding-induced assembly of aligned cellulose nanofibers into ultrastrong and tough bulk materials," *Journal of Materials Chemistry A* 7(47), 27023-27031. DOI: 10.1039/c9ta11118b

Hossain, K. M. Z., Calabrese, V., da Silva, M. A., Schmitt, J., Bryant, S. J., Islam, M. T., Felfel, R. M., Scott, J. L., and Edler, K. J. (2021). "Microstructural, thermal, crystallization, and water absorption properties of films prepared from never-dried and freeze-dried cellulose nanocrystals," *Macromolecular Materials and Engineering* 306(1), article ID 2000462. DOI: 10.1002/mame.202000462

Hou, M., Xu, M., and Li, B. (2018). "Enhanced electrical conductivity of cellulose nanofiber/graphene composite paper with a sandwich structure," *ACS Sustainable Chemistry & Engineering* 6(3), 2983-2990. DOI: 10.1021/acssuschemeng.7b02683

Huang, H. D., Liu, C. Y., Zhou, D., Jiang, X., Zhong, G. J., Yan, D. X., and Li, Z. M. (2015). "Cellulose composite aerogel for highly efficient electromagnetic interference shielding," *Journal of Materials Chemistry A* 3(9), 4983-4991. DOI: 10.1039/c4ta05998k

Islam, M. T., Alam, M. M., Patrucco, A., Montarsolo, A., and Zoccola, M. (2014). "Preparation of nanocellulose: A review," *AATCC Journal of Research* 1(5), 17-23. DOI: 10.14504/ajr.1.5.3

Jiang, F., Li, T., Li, Y., Zhang, Y., Gong, A., Dai, J., Hitz, E., Luo, W., and Hu, L. (2018). "Wood-based nanotechnologies toward sustainability," *Advanced Materials* 30(1), article ID 1703453. DOI: 10.1002/adma.201703453

John, M. J., and Thomas, S. (2008). "Biofibres and biocomposites," *Carbohydrate Polymers* 71(3), 343-364. DOI: 10.1016/j.carbpol.2007.05.040

Karthika, S., Radhakrishnan, T. K., and Kalaichelvi, P. (2016). "A review of classical and nonclassical nucleation theories," *Crystal Growth & Design* 16(11), 6663-6681. DOI: 10.1021/acs.cgd.6b00794

Klemm, D., Heublein, B., Fink, H. P., and Bohn, A. (2005). "Cellulose: Fascinating biopolymer and sustainable raw material," *Angewandte Chemie-International Edition* 44(22), 3358-3393. DOI: 10.1002/anie.200460587

Klemm, D., Kramer, F., Moritz, S., Lindstrom, T., Ankerfors, M., Gray, D., and Dorris, A. (2011). "Nanocelluloses: A new family of nature-based materials," *Angewandte Chemie-International Edition* 50(24), 5438-5466. DOI: 10.1002/anie.201001273

Li, T., Zhang, X., Lacey, S. D., Mi, R., Zhao, X., Jiang, F., Song, J., Liu, Z., Chen, G., Dai, J., *et al.* (2019). "Cellulose ionic conductors with high differential thermal voltage for low-grade heat harvesting," *Nature Materials* 18(6), 608-613. DOI: 10.1038/s41563-019-0315-6

Ling, S., Chen, W., Fan, Y., Zheng, K., Jin, K., Yu, H., Buehler, M. J., and Kaplan, D. L. (2018a). "Biopolymer nanofibrils: Structure, modeling, preparation, and applications," *Progress in Polymer Science* 85, 1-56. DOI: 10.1016/j.progpolymsci.2018.06.004

Ling, S., Kaplan, D. L., and Buehler, M. J. (2018b). "Nanofibrils in nature and materials engineering," *Nature Reviews Materials* 3(4), article no. 18016. DOI: 10.1038/natrevmats.2018.16

Moon, R. J., Martini, A., Nairn, J., Simonsen, J., and Youngblood, J. (2011). "Cellulose nanomaterials review: Structure, properties and nanocomposites," *Chemical Society Reviews* 40(7), 3941-3994. DOI: 10.1039/c0cs00108b

Parthasarathi, R., Bellesia, G., Chundawat, S. P. S., Dale, B. E., Langan, P., and Gnanakaran, S. (2011). "Insights into hydrogen bonding and stacking interactions in cellulose," *Journal of Physical Chemistry A* 115(49), 14191-14202. DOI: 10.1021/jp203620x

Poletto, M., Zattera, A. J., Forte, M. M. C., and Santana, R. M. C. (2012). "Thermal decomposition of wood: Influence of wood components and cellulose crystallite size," *Bioresource Technology* 109, 148-153. DOI: 10.1016/j.biortech.2011.11.122

Ray, S. S., and Bousmina, M. (2005). "Biodegradable polymers and their layered silicate nano composites: In greening the 21st century materials world," *Progress in Materials Science* 50(8), 962-1079. DOI: 10.1016/j.pmatsci.2005.05.002

Segal, L., Creely, J. J., Martin, Jr., A. E., and Conrad, C. M. (1958). "An empirical method for estimating the degree of crystallinity of native cellulose using the X-ray diffractometer," *Textile Research Journal* 29(10), 786-794. DOI: 10.1177/004051755902901003

Song, N., Jiao, D., Cui, S., Hou, X., Ding, P., and Shi, L. (2017). "Highly anisotropic thermal conductivity of layer-by-layer assembled nanofibrillated cellulose/graphene nanosheets hybrid films for thermal management," *ACS Applied Materials & Interfaces* 9(3), 2924-2932. DOI: 10.1021/acsami.6b11979

Swolfs, Y., Verpoest, I., and Gorbatikh, L. (2019). "Recent advances in fibre-hybrid composites: Materials selection, opportunities and applications," *International Materials Reviews* 64(4), 181-215. DOI: 10.1080/09506608.2018.1467365

Thanh, N. T. K., Maclean, N., and Mahiddine, S. (2014). "Mechanisms of nucleation and growth of nanoparticles in solution," *Chemical Reviews* 114(15), 7610-7630. DOI: 10.1021/cr400544s

Thomas, B., Raj, M. C., Athira, K. B., Rubiyah, M. H., Joy, J., Moores, A., Drisko, G. L., and Sanchez, C. (2018). "Nanocellulose, a versatile green platform: From biosources to materials and their applications," *Chemical Reviews* 118(24), 11575-11625. DOI: 10.1021/acs.chemrev.7b00627

Verho, T., Karesoja, M., Das, P., Martikainen, L., Lund, R., Alegria, A., Walther, A., and Ikkala, O. (2013). "Hydration and dynamic state of nanoconfined polymer layers govern toughness in nacre-mimetic nanocomposites," *Advanced Materials* 25(36), 5055-5059. DOI: 10.1002/adma.201301881

Wu, J., Wu, Y., Yang, F., Tang, C., Huang, Q., and Zhang, J. (2019). "Impact of delignification on morphological, optical and mechanical properties of transparent wood," *Composites Part A: Applied Science and Manufacturing* 117, 324-331. DOI: 10.1016/j.compositesa.2018.12.004

Wu, Z., Beltran-Villegas, D. J., and Jayaraman, A. (2020). "Development of a new coarse-grained model to simulate assembly of cellulose chains due to hydrogen bonding," *Journal of Chemical Theory and Computation* 16(7), 4599-4614. DOI: 10.1021/acs.jctc.0c00225

Yan, C., Wang, J., Kang, W., Cui, M., Wang, X., Foo, C. Y., Chee, K. J, and Lee, P. S. (2014). "Highly stretchable piezoresistive graphene-nanocellulose nanopaper for

strain sensors," *Advanced Materials* 26(13), 2022-2027. DOI:
10.1002/adma.201304742

Yang, X., Berthold, F., and Berglund, L. A. (2019). "High-density molded cellulose
fibers and transparent biocomposites based on oriented holocellulose," *ACS Applied
Materials & Interfaces* 11(10), 10310-10319. DOI: 10.1021/acsami.8b22134